

Exact Real Time Dynamics of Quantum Spin Systems Using the Positive-P Representation

R. Ng and E. S. Sørensen

Department of Physics and Astronomy, McMaster University, 1280 Main St W, L8S4LM, Hamilton, ON, Canada

E-mail: ngry@mcmaster.ca

Abstract. We discuss a scheme for simulating the *real time* quantum quench dynamics of interacting quantum spin systems within the positive-P formalism. As model systems we study the transverse field Ising model as well as the Heisenberg model undergoing a quench away from the classical ferromagnetic ordered state and antiferromagnetic Néel state, depending on the sign of the Heisenberg exchange interaction. The connection to the positive-P formalism as it is used in quantum optics is established by mapping the spin operators on to Schwinger bosons. In doing so, the dynamics of the interacting quantum spin system is mapped onto a set of Ito stochastic differential equations (SDEs) the number of which scales *linearly* with the number of spins, N , compared to an exact solution through diagonalization that in the case of the Heisenberg model would require matrices exponentially large in N . This mapping is *exact* and can be extended to higher dimensional interacting systems as well as to systems with an explicit coupling to the environment.

PACS numbers: 05.10.Gg, 75.10.Pq, 75.10.Jm

Submitted to: *J. Phys. A: Math. Gen.*

1. Introduction

The *real time* quantum dynamics following a quench [1–15] is a problem of considerable current interest. Here, our focus is on methods applicable to this problem that are in principle exact (up to controllable errors) and we leave approximate methods aside. Unfortunately, standard quantum Monte Carlo techniques yield results in the imaginary time domain and requires an explicit analytic continuation to access real times, a notoriously difficult procedure. For lattice based models it is possible to perform exact diagonalization but for a N site quantum spin system the size of the Hilbert space is exponential in N , severely limiting the applicability of this method. In recent years methods rooted in the density matrix renormalization group (DMRG) such as TEBD [16] and t-DMRG [17] have been developed to study real-time dynamics of one-dimensional systems. Most recently the infinite size TEBD (iTEBD) has been tuned to yield results for the time dependence of the transverse field Ising model (TFIM) out to relatively large times of order $tJ/\hbar \sim 6 - 10$ [18] as well as in the XXZ and related spin chain models $tJ/\hbar \sim 20$ [5, 9] and often times scales of order $tJ/\hbar \sim 100$ can be accessed [19]. How well such methods will perform in higher dimensions or in the presence of a coupling to the environment is presently a point of intense research and very promising progress have been made [20–23]. Here we investigate an alternative approach for studying the dynamics of interacting quantum spin systems using quantum phase space methods, in particular, the positive-P representation (PPR) [24] of the density operator. As model systems we have studied the one-dimensional transverse field Ising model (TFIM) as well as the Heisenberg model. This approach is quite general and can be extended to higher dimensional interacting quantum spin systems and to open systems with an explicit coupling to the environment.

In general, quantum phase space methods map the dynamics of bosonic operators onto the stochastic evolution of complex phase space variables [24]. Using the positive-P representation, we can easily calculate the expectation values of any normal-ordered products of creation and annihilation operators by calculating the stochastic averages of their equivalent representation in terms of phase-space variables. This is carried out in two steps, first we use Schwinger bosons to replace the Heisenberg spin operators and then employ the positive-P representation. The PPR converts the master equation into a Fokker-Planck equation (FPE) which can then be mapped onto a set of coupled, complex Ito stochastic differential equations (SDEs). The number of SDEs to simulate scales linearly with the number of spins in the system, N , in contrast to an exact diagonalization approach.

To illustrate the feasibility of this approach we study the dynamics of the transverse-field Ising model (TFIM) as well as the isotropic ferromagnetic (FM) Heisenberg model subject to a quantum quench at $T = 0$. The different models are related through the anisotropy parameter, Δ/J . The spin chains are prepared in the ferromagnetic state at $t = 0$ whenever we assume a ferromagnetic Heisenberg model, and evolved by including the

transverse magnetic field term at $t \geq 0$. We calculate the time evolution of the expectation values of the spin operators: $[S^x], [S^y], [S^z]$, which is an average of the individual components over the entire lattice. The averaging is allowed because of the translational symmetry of the system. In addition, we also calculate the results of \hat{S}_z nearest neighbour correlation functions: $[\hat{S}_i^z \hat{S}_{i+1}^z]$ for the TFIM. In order to verify the validity of our results, we in all cases compare them with results from exact diagonalization obtaining excellent agreement.

In a bid to fully take advantage of the PPR, we also attempt to explore finite size effects by simulating lattices sizes of up to 100 spins for the FM isotropic model and 10 spins for the antiferromagnetic (AFM) anisotropic model. Finite size effects are more noticeable in the AFM Hamiltonian and for the latter, the natural choice for an initial state is the classical Néel state.

Since the PPR is well-established in quantum optics, we will relegate the details of the formalism to Appendix A. Readers who are already familiar with the PPR may continue to section 2 where Schwinger bosons are employed to map the spin operators onto bosonic operators. The resulting SDEs are derived in this section with more explicit details layed out in Appendix C. In section 3, the results of the TFIM ($\Delta/J = 0.0$) and the isotropic ($\Delta/J = 1.0$) Heisenberg model are compared with exact diagonalization calculations. We also carry out a brief discussion on the possibility of extending simulation life times by potentially using the gauge-P representation [25] instead. In section 3.1, we present our results for finite size effects in both the anisotropic AFM and the isotropic FM Hamiltonian and discuss our findings. Results and a short discussion on the correlation functions can be found in section 3.2. The conclusion is presented in section 4.

2. Using Schwinger Bosons to derive SDEs

The PPR is based on bosonic coherent states and is only directly applicable to Hamiltonians written in terms of bosonic annihilation and creation operators. In order to apply it to the Heisenberg model or any spin Hamiltonian, we therefore need to rewrite the spin operators in terms of bosonic operators. A convenient way of doing this is by employing the Schwinger boson representation [26,27] and we will demonstrate how it can be applied to the Heisenberg model. A similar approach, based on Schwinger bosons, was previously applied to the study of spontaneous emission non-interacting two-level atoms [28] in quantum optics.

The Heisenberg Hamiltonian with FM ($J > 0$) or AFM interaction ($J < 0$) subject to a quench in the x -direction at $t \geq 0$ is given by:

$$\hat{H} = -J \sum_{\langle i,j \rangle} \hat{\mathbf{S}}_i \cdot \hat{\mathbf{S}}_j - h(t) \sum_i \hat{S}_i^x, \quad h(t) = \begin{cases} h, & t \geq 0 \\ 0, & t < 0 \end{cases} \quad (1)$$

and can be written in terms of the usual raising and lowering operators, $\hat{\mathbf{S}}^\pm = \hat{\mathbf{S}}^x \pm i\hat{\mathbf{S}}^y$. If

we allow anisotropy in the transverse direction[‡], then the Hamiltonian takes the following form

$$\hat{H}_{\text{Heis}} = - \sum_{\langle i,j \rangle} \left[J \hat{S}_i^z \hat{S}_j^z + \Delta \frac{1}{2} (\hat{S}_i^+ \hat{S}_j^- + \hat{S}_i^- \hat{S}_j^+) \right] - \frac{1}{2} h(t) \sum_i \left[\hat{S}_i^+ + \hat{S}_i^- \right] \quad (2)$$

where $\langle i, j \rangle$ indicates nearest-neighbor pairs and Δ/J is a measure of anisotropy. The two models which we first examined were the (i) TFIM ($\Delta/J = 0$):

$$\hat{H}_{\text{TFIM}} = - \sum_{\langle i,j \rangle} \left[J \hat{S}_i^z \hat{S}_j^z \right] - \frac{1}{2} h(t) \sum_i \left[\hat{S}_i^+ + \hat{S}_i^- \right] \quad (3)$$

and the (ii) isotropic Heisenberg model (see Eq. 2) with an anisotropy of $\Delta/J = 1.0$.

The Schwinger boson representation of spins (setting $\hbar = 1$) is given by:

$$\hat{S}^+ \rightarrow \hat{b} \hat{a}^\dagger, \hat{S}^- \rightarrow \hat{b}^\dagger \hat{a}, \hat{S}^z \rightarrow \frac{1}{2} (\hat{a}^\dagger \hat{a} - \hat{b}^\dagger \hat{b}). \quad (4)$$

where \hat{a} and \hat{b} represent two types of bosons and the following commutation relations:

$$\begin{aligned} [\hat{S}^+, \hat{S}^-] &\rightarrow [\hat{a}^\dagger \hat{b}, \hat{b}^\dagger \hat{a}] &&= \hat{a}^\dagger \hat{a} - \hat{b}^\dagger \hat{b} \rightarrow 2\hat{S}^z, \\ [\hat{S}^+, \hat{S}^z] &\rightarrow \left[\hat{a}^\dagger \hat{b}, \frac{1}{2} (\hat{a}^\dagger \hat{a} - \hat{b}^\dagger \hat{b}) \right] &&= -\hat{a}^\dagger \hat{b} \rightarrow -\hat{S}^+, \\ [\hat{S}^-, \hat{S}^z] &\rightarrow \left[\hat{b}^\dagger \hat{a}, \frac{1}{2} (\hat{a}^\dagger \hat{a} - \hat{b}^\dagger \hat{b}) \right] &&= \hat{b}^\dagger \hat{a} \rightarrow \hat{S}^- \end{aligned} \quad (5)$$

demonstrate that the commutation relations of the spin operators are indeed preserved. This is a necessary requirement for a successful mapping. With the Schwinger representation, the two states of a spin-1/2 particle are now described by either an \hat{a} -boson or a \hat{b} -boson per site. A spin-up state: $|\uparrow\rangle$ is the same as having a single \hat{a} -boson whereas a spin down-state: $|\downarrow\rangle$ is the same as having a single \hat{b} -boson. We can therefore replace the spin operators in Eq. 2 and Eq. 3 with the bosonic mapping in Eq. 4 without altering the physics.

As the PPR is well-established[§], we will relegate a brief review of the formalism to Appendix A . Additional technical details pertaining to the specific examples in this paper can be found in Appendix C. For brevity we will present the derivations for only the TFIM (see Eq. 3) where $\Delta/J = 0$.

Using Eq. 4, the equivalent bosonic Hamiltonian for the TFIM is given by

$$\hat{H} = -\frac{J}{4} \sum_{\langle i,j \rangle} \left(\hat{a}_i^\dagger \hat{a}_i \hat{a}_j^\dagger \hat{a}_j - \hat{a}_i^\dagger \hat{a}_i \hat{b}_j^\dagger \hat{b}_j - \hat{b}_i^\dagger \hat{b}_i \hat{a}_j^\dagger \hat{a}_j + \hat{b}_i^\dagger \hat{b}_i \hat{b}_j^\dagger \hat{b}_j \right) - \left(h(t) \sum_i \hat{a}_i^\dagger \hat{b}_i + \hat{b}_i^\dagger \hat{a}_i \right). \quad (6)$$

[‡] The transverse direction is relative to the quantization axis which we have taken to be the z -axis.

[§] See [28–33] for successful applications of the PPR.

Now if we take our system to be closed, its dynamics can be captured via the master equation for the density operator, i.e.

$$\frac{d}{dt}\hat{\rho} = -\frac{i}{\hbar} [\hat{H}, \hat{\rho}], \quad (7)$$

which allows us to use a generalized prescription of the PPR. In principle, it is also possible to calculate open system dynamics by including a Liouvillian term in Eq. 7: $\hat{L}[\hat{\rho}]$, and so this approach is by no means limited to closed system.

To proceed, we first write our density operator in terms of a direct product of projection operators for each site, i.e.

$$\hat{\Lambda}(\vec{\alpha}, \vec{\alpha}^+, \vec{\beta}, \vec{\beta}^+) = \prod_{i=0}^{N-1} \otimes \frac{|\alpha_i\rangle\langle\alpha_i^{+*}|}{\langle\alpha_i^{+*}|\alpha_i\rangle} \otimes \frac{|\beta_i\rangle\langle\beta_i^{+*}|}{\langle\beta_i^{+*}|\beta_i\rangle} \quad (8)$$

where $\vec{\alpha} = (\alpha_0, \dots, \alpha_{N-1})$, $\vec{\alpha}^+ = (\alpha_0^+, \dots, \alpha_{N-1}^+)$, $\vec{\beta} = (\beta_0, \dots, \beta_{N-1})$ and $\vec{\beta}^+ = (\beta_0^+, \dots, \beta_{N-1}^+)$ so that

$$\hat{\rho} = \int P(\vec{\alpha}, \vec{\alpha}^+, \vec{\beta}, \vec{\beta}^+) \hat{\Lambda}(\vec{\alpha}, \vec{\alpha}^+, \vec{\beta}, \vec{\beta}^+) d^2\vec{\alpha} d^2\vec{\alpha}^+ d^2\vec{\beta} d^2\vec{\beta}^+. \quad (9)$$

We can then use the usual correspondence relations (see Eq. A.3) to obtain an FPE (see Eq. A.4) for the PPR distribution function: $P(\vec{\alpha}, \vec{\alpha}^+, \vec{\beta}, \vec{\beta}^+)$. A particular factorization of the diffusion matrix results in a noise matrix which gives us a set of Ito stochastic differential equations for $4N$ of our phase space variables, i.e.

$$\begin{aligned} d\alpha_i &= \left\{ \frac{iJ}{4\hbar} \alpha_i \left[(n_{i+1}^\alpha - n_{i+1}^\beta) + (n_{i-1}^\alpha - n_{i-1}^\beta) \right] + \frac{i\hbar(t)}{2\hbar} \beta_i \right\} dt \\ &+ \frac{1}{2} \sqrt{\frac{iJ}{2\hbar}} \left[\sqrt{\alpha_i \alpha_{i+1}} (dW_{2i}^\alpha + idW_{2i+1}^\alpha) - \sqrt{\alpha_i \alpha_{i-1}} (dW_{2i-2}^\alpha - idW_{2i-1}^\alpha) \right] \\ &+ \frac{i}{2} \sqrt{\frac{iJ}{2\hbar}} \left[\sqrt{\alpha_i \beta_{i-1}} (dW_{2i-2}^{\alpha\beta} + idW_{2i-1}^{\alpha\beta}) - \sqrt{\alpha_i \beta_{i+1}} (dW_{2i}^{\beta\alpha} - idW_{2i+1}^{\beta\alpha}) \right] \end{aligned} \quad (10)$$

$$\begin{aligned} d\beta_i &= \left\{ \frac{iJ}{4\hbar} \beta_i \left[(n_{i+1}^\beta - n_{i+1}^\alpha) + (n_{i-1}^\beta - n_{i-1}^\alpha) \right] + \frac{i\hbar(t)}{2\hbar} \alpha_i \right\} dt \\ &+ \frac{1}{2} \sqrt{\frac{iJ}{2\hbar}} \left[-\sqrt{\beta_i \beta_{i+1}} (dW_{2i}^\beta + idW_{2i+1}^\beta) - \sqrt{\beta_i \beta_{i-1}} (dW_{2i-2}^\beta - idW_{2i-1}^\beta) \right] \\ &+ \frac{i}{2} \sqrt{\frac{iJ}{2\hbar}} \left[-\sqrt{\alpha_{i+1} \beta_i} (dW_{2i}^{\alpha\beta} - idW_{2i+1}^{\alpha\beta}) - \sqrt{\alpha_{i-1} \beta_i} (dW_{2i-2}^{\beta\alpha} + idW_{2i-1}^{\beta\alpha}) \right] \end{aligned} \quad (11)$$

|| The liouvillian term models the effect of the environment on the system

$$\begin{aligned}
d\alpha_i^+ &= \left\{ \frac{iJ}{4\hbar} \alpha_i^+ \left[(n_{i+1}^\beta - n_{i+1}^\alpha) + (n_{i-1}^\beta - n_{i-1}^\alpha) \right] - \frac{ih(t)}{2\hbar} \beta_i^+ \right\} dt \\
&+ \frac{i}{2} \sqrt{\frac{iJ}{2\hbar}} \left[-\sqrt{\alpha_i^+ \alpha_{i+1}^+} (dW_{2i}^{\alpha^+} + idW_{2i+1}^{\alpha^+}) - \sqrt{\alpha_i^+ \alpha_{i-1}^+} (dW_{2i-2}^{\alpha^+} - idW_{2i-1}^{\alpha^+}) \right] \\
&+ \frac{1}{2} \sqrt{\frac{iJ}{2\hbar}} \left[-\sqrt{\alpha_i^+ \beta_{i-1}^+} (dW_{2i-2}^{\alpha^+ \beta^+} + idW_{2i-1}^{\alpha^+ \beta^+}) - \sqrt{\alpha_i^+ \beta_{i+1}^+} (dW_{2i}^{\beta^+ \alpha^+} - idW_{2i+1}^{\beta^+ \alpha^+}) \right] \quad (12)
\end{aligned}$$

$$\begin{aligned}
d\beta_i^+ &= \left\{ \frac{iJ}{4\hbar} \beta_i^+ \left[(n_{i+1}^\alpha - n_{i+1}^\beta) + (n_{i-1}^\alpha - n_{i-1}^\beta) \right] - \frac{ih(t)}{2\hbar} \alpha_i^+ \right\} dt \\
&+ \frac{i}{2} \sqrt{\frac{iJ}{2\hbar}} \left[-\sqrt{\beta_i^+ \beta_{i+1}^+} (dW_{2i}^{\beta^+} + idW_{2i+1}^{\beta^+}) - \sqrt{\beta_i^+ \beta_{i-1}^+} (dW_{2i-2}^{\beta^+} - idW_{2i-1}^{\beta^+}) \right] \\
&+ \frac{1}{2} \sqrt{\frac{iJ}{2\hbar}} \left[-\sqrt{\alpha_{i+1}^+ \beta_i^+} (dW_{2i}^{\alpha^+ \beta^+} - idW_{2i+1}^{\alpha^+ \beta^+}) - \sqrt{\alpha_{i-1}^+ \beta_i^+} (dW_{2i-2}^{\beta^+ \alpha^+} + idW_{2i-1}^{\beta^+ \alpha^+}) \right], \quad (13)
\end{aligned}$$

where $i = 0 \dots N - 1$ labels the vector components and we have defined $n_i^\alpha = \alpha_i^+ \alpha_i$ and $n_i^\beta = \beta_i^+ \beta_i$, which are complex phase space functions representing the number of \hat{a} and \hat{b} -bosons (per site i) respectively. With this particular choice of noise matrix, we have introduced eight $2N \times 1$ Wiener increment vectors with the usual statistical properties that $\langle dW_i^x dW_j^y \rangle = dt \delta_{xy} \delta_{ij}$ and $\langle dW_i^x \rangle = 0$, where $i = 0 \dots N - 1$ and $x, y = \alpha, \alpha^+, \beta, \beta^+, \beta\alpha, \alpha\beta, \beta^+\alpha^+, \alpha^+\beta^+$ labels each Wiener increment vector. We would like to point out that the subscript labels of the Wiener increment vector are not unique and the labeling scheme[¶] was chosen simply for convenience (see Appendix C).

2.1. Inclusion of Anisotropy

Had we begun with the full anisotropic Hamiltonian in Eq. 2 instead and carried out the same steps as in section 2, it can be shown that anisotropy is included by adding the following expressions into the drift terms of Eq. 10 to Eq. 13:

$$d\alpha_i \sim + \frac{i\Delta}{2\hbar} \beta_i (m_{i-1} + m_{i+1}) dt \quad (14)$$

$$d\beta_i \sim + \frac{i\Delta}{2\hbar} \alpha_i (m_{i-1}^+ + m_{i+1}^+) dt \quad (15)$$

$$d\alpha_i^+ \sim - \frac{i\Delta}{2\hbar} \beta_i^+ (m_{i-1}^+ + m_{i+1}^+) dt \quad (16)$$

$$d\beta_i^+ \sim - \frac{i\Delta}{2\hbar} \alpha_i^+ (m_{i-1}^+ + m_{i+1}^+) dt \quad (17)$$

[¶] Note that with the inclusion of periodic boundary conditions: $\alpha_{-1} \rightarrow \alpha_{N-1}$ and $\alpha_N \rightarrow \alpha_0$. However since there are $2N \times 1$ Wiener increments, then it is periodic in $2N$ instead. For e.g. $dW_{-1}^x = dW_{2N-1}^x$ and $dW_{2N}^x = 0$.

where the following shorthand $m_i = \alpha_i \beta_i^+$, $m_i^+ = \alpha_i^+ \beta_i$ was used. For the stochastic terms however, only the mixed derivative diffusion terms (i.e. those containing $\alpha\beta$ and $\alpha^+\beta^+$) are modified in the following way

$$d\alpha_i \sim + \frac{i}{2} \sqrt{\frac{i}{2\hbar}} \left[-\sqrt{J\alpha_i\beta_{i-1} - 2\Delta\beta_i\alpha_{i-1}}(\dots\dots) - \sqrt{J\alpha_i\beta_{i+1} - 2\Delta\alpha_{i+1}\beta_i}(\dots\dots) \right] \quad (18)$$

$$d\beta_i \sim + \frac{i}{2} \sqrt{\frac{i}{2\hbar}} \left[-\sqrt{J\beta_i\alpha_{i+1} - 2\Delta\beta_{i+1}\alpha_i}(\dots\dots) - \sqrt{J\beta_i\alpha_{i-1} - 2\Delta\alpha_i\beta_{i-1}}(\dots\dots) \right] \quad (19)$$

$$d\alpha_i^+ \sim + \frac{i}{2} \sqrt{\frac{i}{2\hbar}} \left[-\sqrt{J\beta_{i-1}^+\alpha_i^+ - 2\Delta\beta_i^+\alpha_{i-1}^+}(\dots\dots) - \sqrt{J\beta_{i+1}^+\alpha_i^+ - 2\Delta\alpha_{i+1}^+\beta_i^+}(\dots\dots) \right] \quad (20)$$

$$d\beta_i^+ \sim + \frac{i}{2} \sqrt{\frac{i}{2\hbar}} \left[-\sqrt{J\beta_i^+\alpha_{i-1}^+ - 2\Delta\beta_{i-1}^+\alpha_i^+}(\dots\dots) - \sqrt{J\beta_i^+\alpha_{i+1}^+ - 2\Delta\alpha_i^+\beta_{i+1}^+}(\dots\dots) \right] \quad (21)$$

where the terms in $(\dots\dots)$ represent the same Wiener increment combinations as in Eq. 10 to 13. The Ito SDEs we have derived are able to describe other types of spins models such as the XY model and the XYZ model (to name a few), just by adjusting or including a few parameters. For the last two cases, we would have to take a trivial generalization in the derivations by introducing two different anisotropy terms in Eq. 2. An informative review article on the the quantum quench dynamics of other variants of the Heisenberg Hamiltonian using other numerical methods can be found in [9].

3. Results and Discussion

To test our formalism, we first simulated the FM ($J > 0$) spin Hamiltonian for the TFIM ($\Delta/J = 0$) and the isotropic Heisenberg Hamiltonian ($\Delta/J = 1.0$) in Eq. 2 for high ($h/J = 10$) and low ($h/J = 0.5$) field values. This was compared to results from exact diagonalization calculations using a small system with $N = 4$ spins. The Stratanovich version of the SDES⁺ in Eq. 10 to Eq. 13 were simulated using a semi-implicit Stratanovich algorithm as they are known to exhibit superior convergence properties [34]. To track the dynamics of the system, we calculated the expectation values of all three spin components at each site i : $\langle S_i^x \rangle$, $\langle S_i^y \rangle$, $\langle S_i^z \rangle$. Using the translation symmetry of the system, we further averaged them over the entire lattice to obtain an average expectation value of the spin components per site: $[S^x]$, $[S^y]$, $[S^z]$. These expectation values were calculated using the stochastic averages of their respective phase space functions, i.e.

$$[S^x] = \sum_{i=0}^{N-1} \left\langle \frac{1}{2} (\hat{a}_i^\dagger \hat{b}_i + \hat{b}_i^\dagger \hat{a}_i) \right\rangle = \sum_{i=0}^{N-1} \left\langle \frac{1}{2} (\alpha_i^+ \beta_i + \beta_i^+ \alpha_i) \right\rangle, \quad (22)$$

⁺ The Stratanovich correction terms worked out to be zero and hence the Stratanovich form of the SDEs from Eq. 10 to Eq. 13 have the exact same form as the derived Ito SDEs.

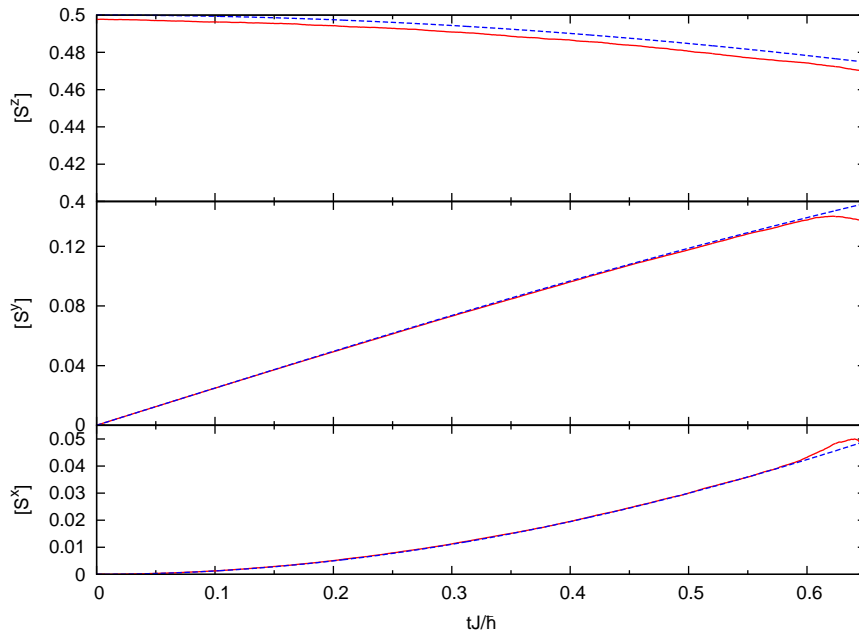


Figure 1. TFIM following a transverse quench. From top to bottom: plots of $[S^x]$, $[S^y]$, $[S^z]$ vs tJ/\hbar respectively. The stochastic averages, $\langle\langle \cdot \rangle\rangle$ are given by red solid lines while exact diagonalization results are represented by the green dashed lines. Simulation parameters: $N = 4$, $n_{traj} = 10^6$, $dt = 0.001$, $h/J = 0.5$, $\Delta/J = 0.0$. Agreement remains good till approximately $tJ/\hbar = 0.6$.

$$[S^y] = \sum_{i=0}^{N-1} \langle \frac{1}{2i} (\hat{a}_i^\dagger \hat{b}_i - \hat{b}_i^\dagger \hat{a}_i) \rangle = \sum_{i=0}^{N-1} \langle \langle \frac{1}{2i} (\alpha_i^+ \beta_i - \beta_i^+ \alpha_i) \rangle \rangle, \quad (23)$$

$$[S^z] = \sum_{i=0}^{N-1} \langle \frac{1}{2} (\hat{a}_i^\dagger \hat{a}_i - \hat{b}_i^\dagger \hat{b}_i) \rangle = \sum_{i=0}^{N-1} \langle \langle \frac{1}{2} (\alpha_i^+ \alpha_i - \beta_i^+ \beta_i) \rangle \rangle, \quad (24)$$

where $\langle\langle \cdot \rangle\rangle$ denotes a stochastic average.

The initial state of the system was taken to be the classical ferromagnetic state: $|\uparrow\uparrow \dots \uparrow\rangle$ and the dynamics were observed for $t \geq 0$ during which a transverse field is turned on. The results for the TFIM are shown in Fig. 1 and Fig. 2 for different field strengths while the results for the isotropic ($\Delta/J = 1.0$) model are shown in Fig. 3 and Fig. 4. Both models show good agreement with exact diagonalization calculations.

The only drawback of the PPR is that the simulations are usually valid only for relatively short lifetimes (roughly $tJ/\hbar \sim 0.45 - 0.65$ for the models examined) before sampling errors caused by diverging trajectories take over. In Fig. 1 for example, the onset of the effects of diverging trajectories can be seen at around $tJ/\hbar \sim 0.58$ where a deviation of the SDE results and exact calculations begin to appear. However, for the time scales where the simulations

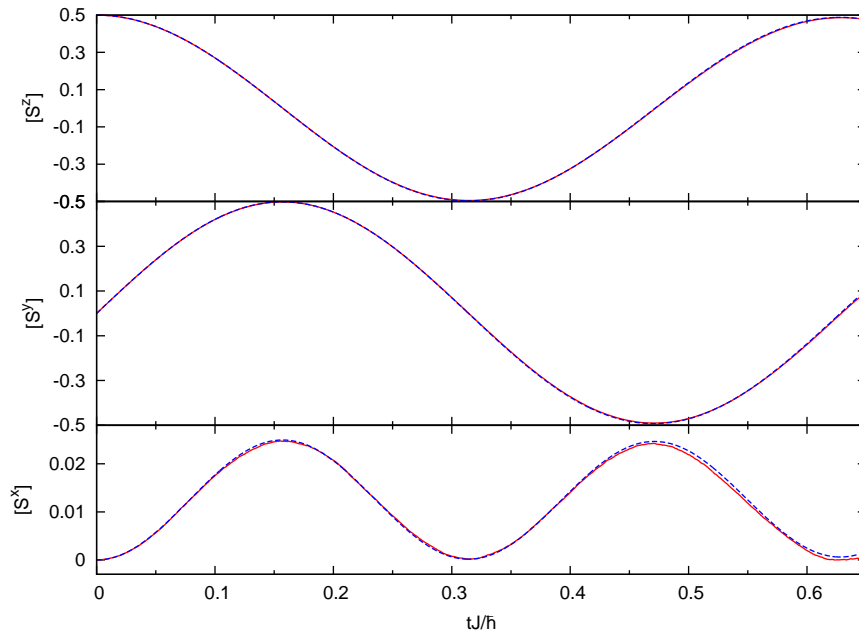


Figure 2. TFIM following a transverse quench. From top to bottom: plots of $[S^x]$, $[S^y]$, $[S^z]$ vs tJ/\hbar respectively. The stochastic averages, $\langle\langle \cdot \rangle\rangle$ are given by red solid lines while exact diagonalization results are represented by the green dashed lines. Simulation parameters: $N = 4$, $n_{traj} = 2 \times 10^5$, $dt = 0.001$, $h/J = 10.0$, $\Delta/J = 0.0$. Agreement remains good till approximately $tJ/\hbar = 0.65$.

remain finite, it does yield good results.

One should not be alarmed as this is a common problem associated in using the PPR and can be attributed to the nature of the SDEs derived and not due to a non-converging numerical algorithm [35–37]. In fact, Deuar [38] examined this issue when applying the PPR to the exact dynamics of many-body systems. If we abide by Deuar’s findings strictly, we see that there are no drift and noise divergences present in the SDEs in Eq. 10–13. However, we suspect drift terms of the form $\sim iX_i \left[(\mp n_{i+1}^\alpha \pm n_{i+1}^\beta) + (n_{i-1}^\alpha \pm n_{i-1}^\beta) \right]$, where $X_i = \alpha_i, \alpha_i^+, \beta, \beta^+$ can be problematic. This is because if we take into consideration the translational symmetry of the system, then we can approximately say that

$$iX_i \left[\left(\mp n_{i+1}^\alpha \pm n_{i+1}^\beta \right) + \left(\mp n_{i-1}^\alpha \pm n_{i-1}^\beta \right) \right] \approx 2iX_i \left(\mp n_i^\alpha \pm n_i^\beta \right), \quad (25)$$

which now clearly exhibits offending terms [38] that cause trajectories to escape to infinity, since $dX_i \sim X_i^2 [\dots] dt + \dots$

The gauge-P representation [25, 37–40] was developed to specifically deal with such drift instabilities. In the gauge-P representation, arbitrary gauge functions, $\{g_k\}$ can be introduced into the SDEs whose effect is a modification of the deterministic evolution. This

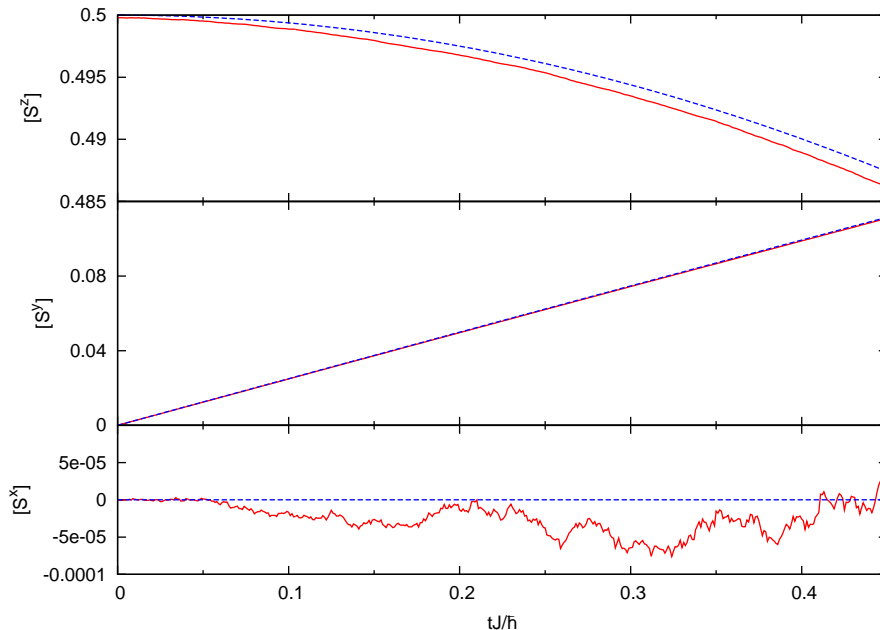


Figure 3. Isotropic Heisenberg model following a transverse quench. From top to bottom: plots of $[S^x]$, $[S^y]$, $[S^z]$ vs tJ/\hbar respectively. The stochastic averages, $\langle\langle \cdot \rangle\rangle$ are given by red solid lines while exact diagonalization results are represented by green dashed lines. Simulation parameters: $N = 4$, $n_{traj} = 10^6$, $dt = 0.001$, $h/J = 0.5$, $\Delta/J = 1.0$. Agreement remains good and both results are nearly indistinguishable. The simulations diverge at approximately $tJ/\hbar = 0.45$.

can be done at the expense of introducing another stochastic variable (Ω), in $\hat{\Lambda}$, which manifests itself as a weight term when calculating stochastic averages. To be more specific using the gauge-P representation [25], the Ito SDEs are altered such that:

$$d\alpha_i = (A_i^+ - g_k B_{jk}) dW_k \quad (26)$$

$$d\Omega = \Omega (V dt + g_k dW_k) \quad (27)$$

where summation over k is implied and V is the constant term that may appear after substituting the correspondence relations into an equation of motion for $\hat{\rho}$.

The gauge-P representation has been very successful in simulating the dynamics of many-mode bose gases [41–43] partly because such systems result in neat diagonal noise matrices that are easier to handle as seen in Eq. 26. However, it is evidently not as straightforward to apply it in our case as we have a much more complicated non-diagonal noise matrix. The true complication arises when we attempt to calculate Stratonovich correction terms as it is the Stratonovich version of the SDEs that are simulated. We believe that the application of the gauge-P is possible in principle but requires a bit more thought for Heisenberg systems if using the Schwinger boson approach.

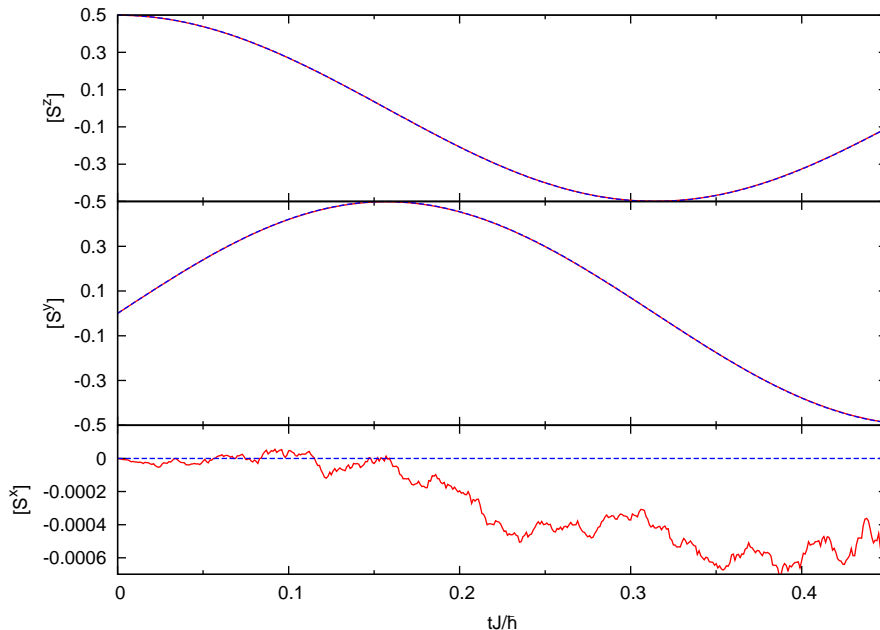


Figure 4. Isotropic Heisenberg model following a transverse quench. From top to bottom: plots of $[S^x]$, $[S^y]$, $[S^z]$ vs tJ/\hbar respectively. The stochastic averages, $\langle\langle \cdot \rangle\rangle$ are given by red solid lines while exact diagonalization results are represented by green dashed lines. Simulation parameters: $N = 4$, $n_{traj} = 10^5$, $dt = 0.001$, $\hbar/J = 10.0$, $\Delta/J = 1.0$. Agreement remains good and both results are nearly indistinguishable. The simulations diverge at approximately $tJ/\hbar = 0.45$.

3.1. Finite size effects

The main advantage of the PPR is the linear scaling with the number of spins, N , as compared to the exponentially large matrices needed for an exact solution. We first demonstrate the capabilities of the PPR at simulating large system sizes by showing results for the FM isotropic Heisenberg case at a field value of $\hbar/J = 10$, prepared in the initial FM state as in Fig. 4. As expected, we do not observe any finite size effects within the life time of the stochastic simulations. Even with a chain consisting of 100 spins (Fig. 5), the dynamics exhibited are similar to that of a four-spin chain. The simulations are compared against the exact diagonalization results for an $N = 4$ system and exhibit identical real time evolution of the spin components for a 1D chain with FM interactions, i.e. finite size effects are negligible.

This is not the case for a 1D AFM ($J < 0$) however. A quantum quench in this model with $\hbar = 0$ starting from the Néel state has previously been extensively studied [5]. In order to verify that in our approach finite size effects do exist, we performed $N = 4$ and $N = 10$ exact calculations for the anisotropic AFM with different values of anisotropy: Δ/J . Two

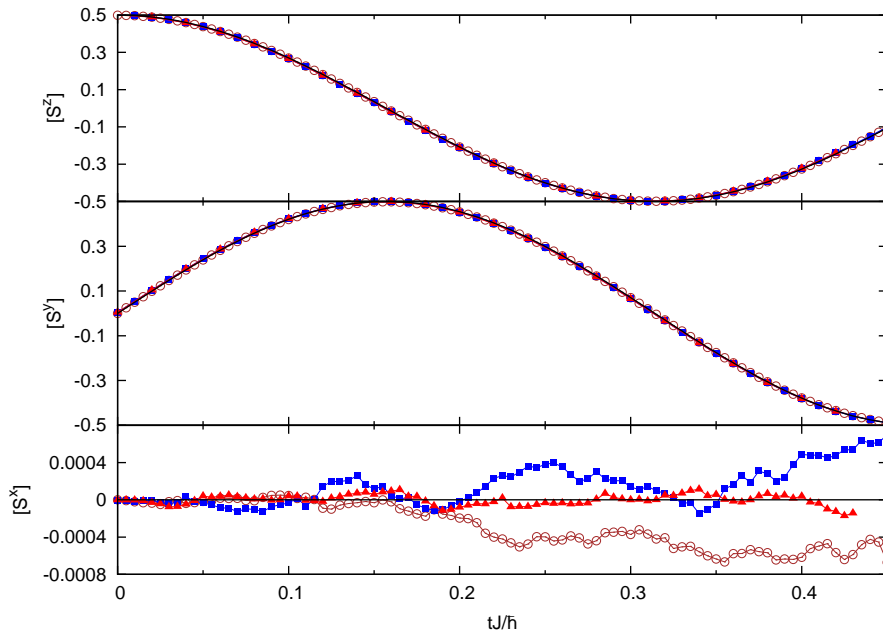


Figure 5. Isotropic Heisenberg model following a transverse-field quench at $tJ/\hbar = 0$ from $h/J = 0.0$ to $h/J = 10.0$, beginning in the FM ground state: $|\uparrow\uparrow\dots\uparrow\rangle$. FM interactions assumed: $sign(J) = +1$. From top to bottom: plots of $[S^x]$, $[S^y]$, $[S^z]$ vs tJ/\hbar respectively. The stochastic averages, $\langle\langle.\rangle\rangle$ are for $N = 4$: (\blacksquare), $N = 10$: (\circ), $N = 100$: (\blacktriangle), while exact diagonalization results for $N = 4$ are represented by the black solid line. Simulation parameters: $n_{traj}^{(N=4)} = 10^5$, $n_{traj}^{(N=10)} = 2 \times 10^5$, $n_{traj}^{(N=100)} = 5 \times 10^4$, $dt = 0.001$, $\Delta/J = 1.0$. Agreement remains good and finite size effects are negligible. The simulations diverge at approximately $tJ/\hbar \sim 0.45$.

sample exact calculations are shown in Fig. 6 and Fig. 7 respectively for $\Delta/J = -0.8$ and $\Delta/J = -1.5$ for low field values of $h/J = 0.5$. For the AFM Heisenberg Hamiltonian, the system is initialized in the classical AFM Néel state: $|\uparrow\downarrow\dots\uparrow\downarrow\rangle$.

An immediate observation is that increasing the value of Δ , reduces the time: t_{finite} , which we define as the time that significant finite size effects are noticeable. A natural progression to make in order to take advantage of the SDES we have derived, is to increase the value Δ/J till $t_{finite} < t_{life}$, thereby allowing us to explore the finite size effects of macroscopically large systems.

We observe finite size effects through the same observables as in eq. 22 to eq. 24. However for the initial Néel state, it is more meaningful to take into consideration the alternating

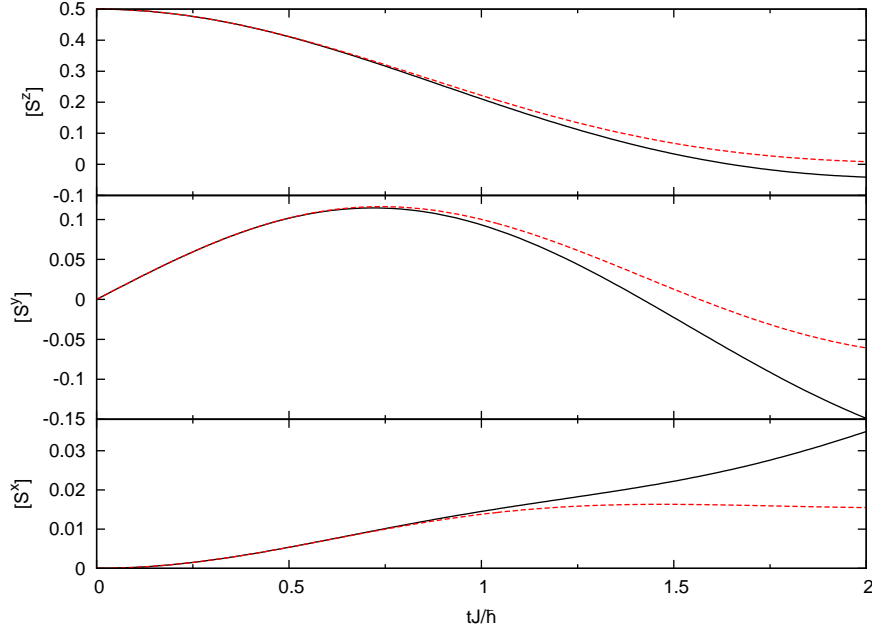


Figure 6. Anisotropic Heisenberg model following a transverse-field quench at $tJ/\hbar = 0$ from $h/J = 0.0$ to $h/J = 10.0$, beginning in the AFM Neel state: $|\uparrow\downarrow \dots \uparrow\downarrow\rangle$. AFM interactions assumed: $sign(J) = -1$. From top to bottom: plots of $[S^x]$, $[S^y]$, $[S^z]$ vs tJ/\hbar respectively. The exact calculations for the $N = 4$ (solid black lines) and $N = 10$ (dashed red lines) are compared. We observe $t_{finite}J/\hbar \sim 0.8$ for $\Delta/J \sim -0.8$

sign of spins when calculating the averaged spin components*, i.e.:

$$[S^x] = \sum_{i=0}^{N-1} \langle \frac{1}{2}(\hat{a}_i^\dagger \hat{b}_i + \hat{b}_i^\dagger \hat{a}_i) \rangle = \sum_{i=0}^{N-1} \langle \langle \frac{1}{2}(\alpha_i^+ \beta_i + \beta_i^+ \alpha_i) \rangle \rangle, \quad (28)$$

$$[S^y] = \sum_{i=0}^{N-1} \langle \frac{1}{2i}(-1)^i(\hat{a}_i^\dagger \hat{b}_i - \hat{b}_i^\dagger \hat{a}_i) \rangle = \sum_{i=0}^{N-1} (-1)^i \langle \langle \frac{1}{2i}(\alpha_i^+ \beta_i - \beta_i^+ \alpha_i) \rangle \rangle, \quad (29)$$

and

$$[S^z] = \sum_{i=0}^{N-1} \langle \frac{1}{2}(-1)^i(\hat{a}_i^\dagger \hat{a}_i - \hat{b}_i^\dagger \hat{b}_i) \rangle = \sum_{i=0}^{N-1} (-1)^i \langle \langle \frac{1}{2}(\alpha_i^+ \alpha_i - \beta_i^+ \beta_i) \rangle \rangle. \quad (30)$$

Increasing Δ/J however has the adverse effect of decreasing t_{life} significantly. Thus while it is possible to simulate macroscopically large system sizes, we find that the SDE simulations diverge much sooner than t_{finite} . Fig. 8 ($\Delta/J = -0.5$, $h/J = 10.0$) reinforces our claim that t_{finite} decreases with Δ/J as no finite size effects are observed up to $tJ/\hbar = 1$, in sharp

* Note that there is an exception. There is no need to account for a sign change for the observable: $[S_x]$

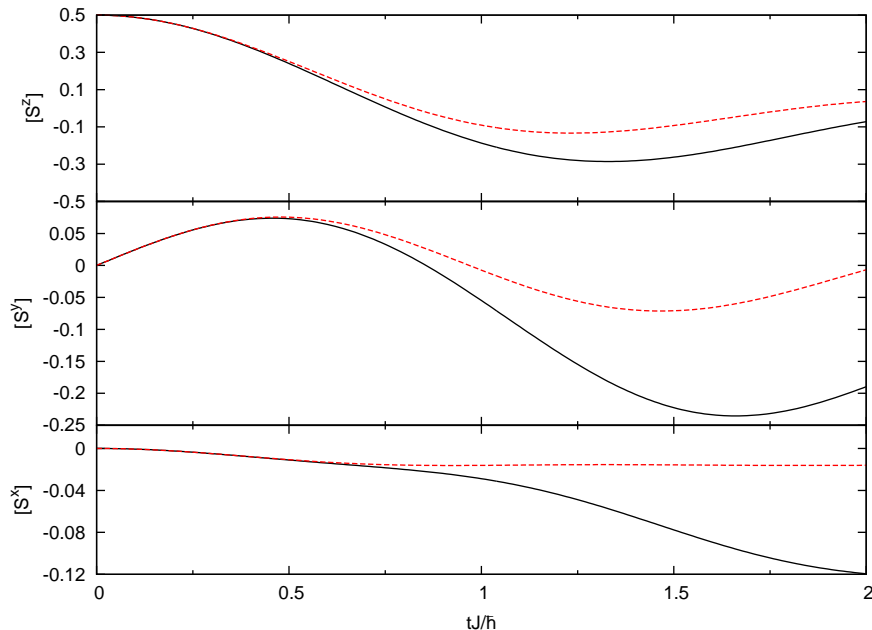


Figure 7. Anisotropic Heisenberg model following a transverse-field quench at $tJ/\hbar = 0$ from $h/J = 0.0$ to $h/J = 10.0$, beginning in the AFM Neel state: $|\uparrow\downarrow \dots \uparrow\downarrow\rangle$. AFM interactions assumed: $sign(J) = -1$. From top to bottom: plots of $[S^x]$, $[S^y]$, $[S^z]$ vs tJ/\hbar respectively. The exact calculations for the $N = 4$ (solid black lines) and $N = 10$ (dashed red lines) are compared. We observe $t_{finite}J/\hbar \sim 0.5$ for a given anisotropy of $\Delta/J \sim -1.5$

comparison to Fig. 6 ($\Delta/J = -0.8$) and Fig. 7 ($\Delta/J = -1.5$), albeit for $h/J = 0.5$. Our last effort to observe finite size effects was to increase Δ/J to -0.8 with hopes that $t_{life} > t_{finite}$. As seen in Fig. 9, our simulations do not survive beyond t_{finite} . Since t_{finite} depends on the anisotropy Δ/J , increasing the system size while possible will result in t_{life} of the same order. In general, we find that increasing Δ/J will *decrease* t_{life} as well as t_{finite} such that $t_{life} < t_{finite}$ always holds true. This thwarts our efforts on examining finite size effects for the AFM case. Furthermore, we find that using an initial Neel state results in poor convergence for the observable: $[S^x]$ as seen in Fig. 8 (and even more so in Fig. 9) compared to an initial FM ground state and it is likely that we have used an insufficient number of trajectories in our simulations. Nevertheless, we have demonstrated the applicability of the PPR to AFM systems.

3.2. Nearest neighbor correlation functions

Correlation functions are generally of greater interest seeing as they are experimentally accessible quantities. In order to demonstrate the applicability of the PPR in this respect, we calculate the nearest neighbour spin correlation functions for the z-component, which is

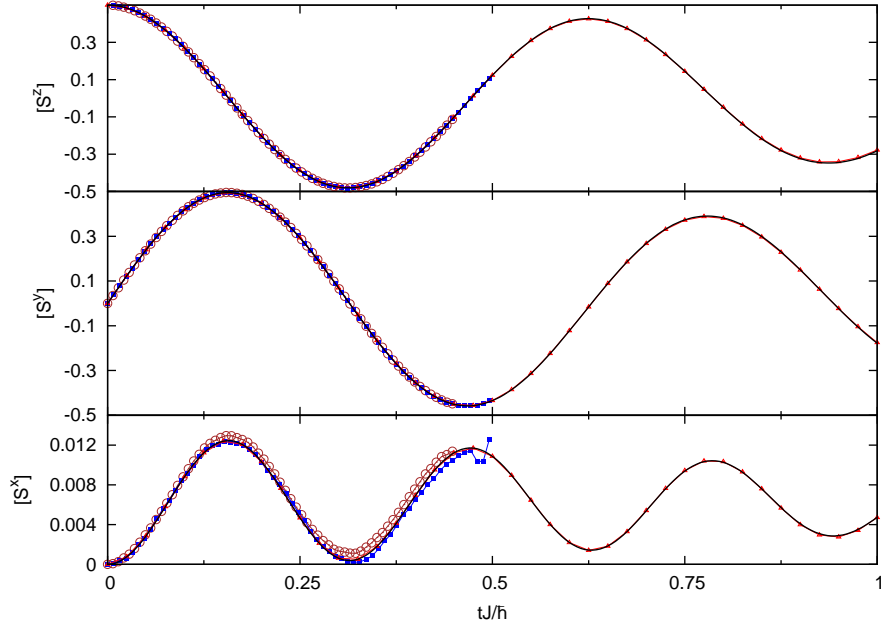


Figure 8. Anisotropic Heisenberg model following a transverse-field quench at $tJ/\hbar = 0$ from $h/J = 0.0$ to $h/J = 10.0$, beginning in the AFM ground state: $|\uparrow\downarrow \dots \uparrow\downarrow\rangle$. AFM interactions assumed: $\text{sign}(J) = -1$. From top to bottom: plots of $[S^x]$, $[S^y]$, $[S^z]$ vs tJ/\hbar respectively. The stochastic averages, $\langle\langle \cdot \rangle\rangle$ are for $N = 4$: (—■—) and $N = 10$: (—○—), while exact diagonalization results are for $N = 4$: (black solid lines) and $N = 10$: (—▲—). Simulation parameters: $n_{\text{traj}}^{(N=4)} = 10^6$, $n_{\text{traj}}^{(N=10)} = 10^5$, $dt = 0.001$, $\Delta/J = -0.5$. Agreement remains good and finite size effects are unnoticeable up to $tJ\hbar = 1$. The SDEs diverge at $t_{\text{life}}J/\hbar \sim 0.48$.

defined as:

$$\left[\hat{S}_i^z \hat{S}_{i+1}^z \right] = \sum_{i=0}^{N-1} \frac{\langle \hat{S}_i^z \hat{S}_{i+1}^z \rangle}{N} = \frac{1}{4} \sum_{i=0}^{N-1} \frac{\langle\langle (n_i^\alpha - n_i^\beta) (n_{i+1}^\alpha - n_{i+1}^\beta) \rangle\rangle}{N}, \quad (31)$$

where periodic boundary conditions apply and as before, the following shorthand has been used: $n_i^\alpha = \alpha_i^+ \alpha_i$, $n_i^\beta = \beta_i^+ \beta_i$. Our calculations in Fig. 10 compares the stochastic averages of correlation functions with the results from exact diagonalization. It is because the correlation function shows poorer convergence than the spin components that we include errorbars for this calculation. Error bars can be calculated from a simple binning analysis of the trajectories and applying the central limit theorem [32]. It is not surprising to find poorer convergence for the correlation functions since they amount to higher order moments of the complex phase space variables. Due to the noise terms in the SDEs, the phase space variables are exponentials of gaussian random numbers which are known to diverge sooner for higher moments.

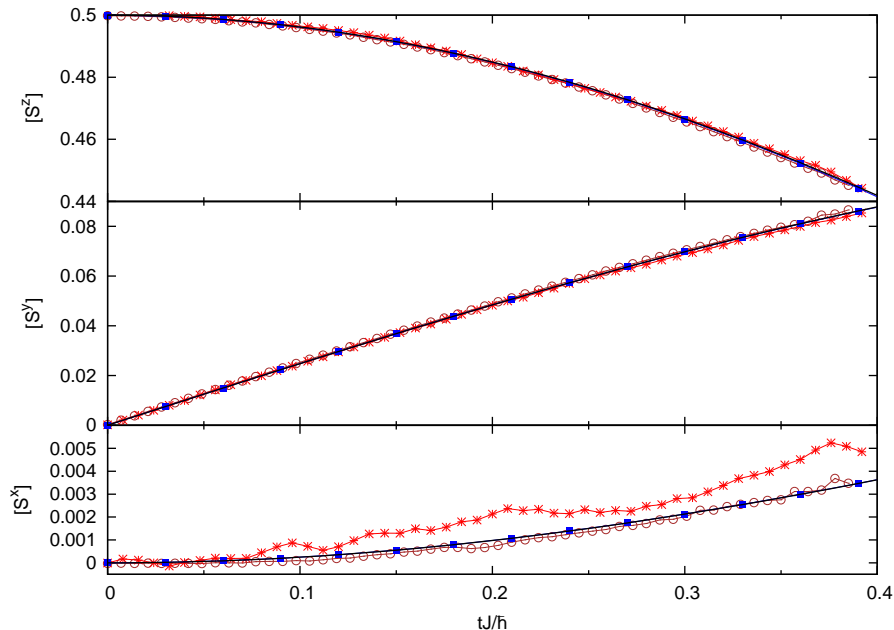


Figure 9. Anisotropic Heisenberg model following a transverse-field quench at $tJ/\hbar = 0$ from $h/J = 0.0$ to $h/J = 0.5$, beginning in the AFM ground state: $|\uparrow\downarrow \dots \uparrow\downarrow\rangle$. AFM interactions assumed: $\text{sign}(J) = -1$. From top to bottom: plots of $[S^x]$, $[S^y]$, $[S^z]$ vs tJ/\hbar respectively. The stochastic averages, $\langle\langle \cdot \rangle\rangle$ are for $N = 4$: (—○—) and $N = 10$: (—*—), while exact diagonalization results are for $N = 4$: (black solid lines) and $N = 10$: (—■—). Simulation parameters: $n_{\text{traj}}^{(N=4)} = 10^6$, $n_{\text{traj}}^{(N=10)} = 10^5$, $dt = 0.001$, $\Delta/J = -0.8$. Finite size effects are unnoticeable at $t_{\text{life}}J/\hbar \sim 0.4$.

4. Conclusion

We have shown how the real-time quantum quench dynamics of spin systems can be simulated via the use of SDEs. This was done by writing the Heisenberg spin operators in terms of Schwinger bosons and deriving a Fokker-Planck Equation using the PPR for the density operator. This in turns allows us to obtain Ito stochastic differential equations which can be used to calculate the expectation values of normally ordered bosonic operators. An attractive feature of this prescription is that the number of SDEs scale linearly as N and can in principle be used to simulate macroscopic system sizes. In addition, our method is generalizable to higher dimensions and other geometries as well and explicit couplings to the environment can be included.

The main drawback of the positive-P representation, however is its notoriously short life time which prevents us from obtaining useful results beyond a certain time: t_{life} . For the TFIM and the anisotropic Heisenberg model, we found a bare application of the PPR to have $t_{\text{life}}J/\hbar \sim 0.45 - 0.65$. We suspect that this is due to drift instability terms present

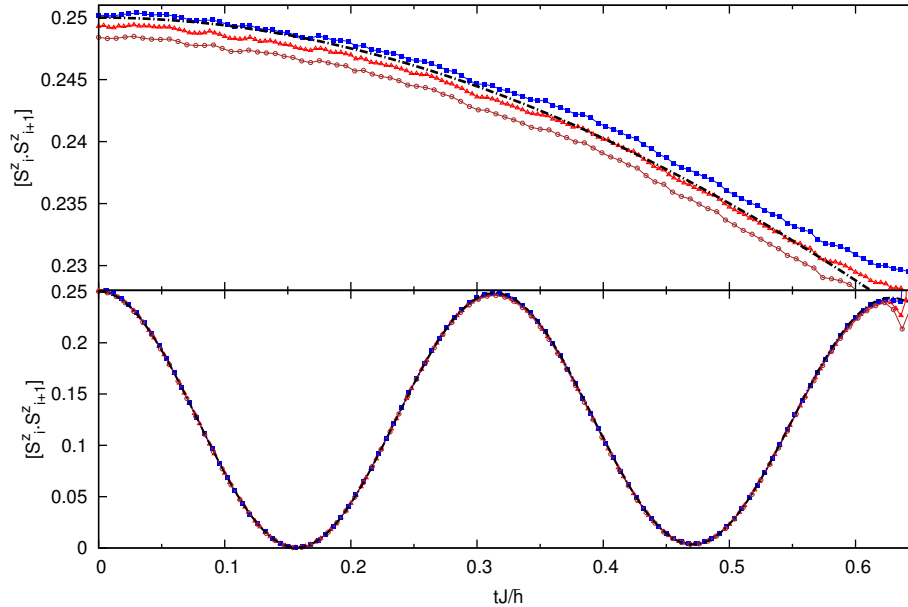


Figure 10. TFIM following a transverse-field quench at $tJ/\hbar = 0$ from $h/J = 0.0$ to $h/J = 0.5$ (top) and $h/J = 0.0$ to $h/J = 10.0$ (bottom) beginning in the FM ground state: $|\uparrow\uparrow \dots \uparrow\uparrow\rangle$. FM interactions assumed: $sign(J) = 1$. Plots of $[\hat{S}_i^z \hat{S}_{i+1}^z]$ vs tJ/\hbar respectively. The stochastic averages, $\langle\langle \cdot \rangle\rangle$ for $N = 4$ are represented by solid red lines (—▲—) while the averages plus and minus one standard deviation are presented by (—■—) and (—○—) lines respectively. Exact diagonalization results are given by dot-dashed black curves. Simulation parameters: $n_{traj} = 10^6$, $dt = 0.001$, $\Delta/J = 0.0$.

in the SDEs that cause trajectories to diverge within this time scale.

We also attempted to explore finite size effects which were more significant for the anisotropic AFM Hamiltonian beginning in the classical Néel state. For the FM case, no finite size effects were observed even for a lattice size of 100 spins within its lifetime. We find that the more negative the anisotropy parameter in the AFM Hamiltonian, the sooner finite size effects are observed, i.e. t_{finite} decreases. However, this has the adverse effect of decreasing t_{life} such that $t_{life} < t_{finite}$ for the simulations that we have carried out.

Finally, we would like to point that in cases where the underlying Hamiltonian has conserved properties, such as the models addressed in this paper, then it could be advantageous to use projection methods instead [44, 45]. This ensures the use of a more efficient basis set which will lead to improved simulation performances. In particular, there exists the PPR approach uses the $SU(n)$ spin coherent states [46] as a basis set instead.

An obvious future direction of our research involves applying the gauge-P representation in a bid to extend simulation life times and to examine the efficiency of the other methods

suggested above. Also the study of systems in higher dimensions with and without couplings to the environment would be of considerable interest.

Appendix A. The positive-P representation

In this section, we will review the positive-P representation [24] that has been applied to both quantum optics [28–30] and exact many-body simulations of bose-gases [33, 47–49] successfully. The PPR is already well established and our aim for including this review is simply to provide a self-contained paper for readers who are not as familiar with it.

In short, the PPR is an expansion of the density operator in terms of an off-diagonal coherent state basis:

$$\hat{\rho} = \int P(\alpha, \alpha^+) \hat{\Lambda}(\alpha, \alpha^+) d^2\alpha d^2\alpha^+ = \int P(\alpha, \alpha^+) \frac{|\alpha\rangle\langle\alpha^{+*}|}{\langle\alpha^{+*}|\alpha\rangle} d^2\alpha d^2\alpha^+ \quad (\text{A.1})$$

where $|\alpha\rangle = e^{-\frac{1}{2}|\alpha|^2} \sum_{n=0}^{\infty} \frac{\alpha^n}{n!} |n\rangle$ is the standard bosonic coherent state [50] that are eigenstates of the annihilation operator \hat{a} . $P(\alpha, \alpha^+)$ plays the role of a distribution function in the phase space spanned by $\{\alpha, \alpha^+\}$ and can be chosen such that it remains real and positive. In addition, due to the normalization factor in the denominator of Eq. A.1 and using the fact that $\text{Tr}[\hat{\rho}] = 1$, we see that

$$\int P(\alpha, \alpha^+) d^2\alpha d^2\alpha^+ = 1 \quad (\text{A.2})$$

i.e. the distribution is normalized over the entire complex phase space. Simply put, we can interpret $P(\alpha, \alpha^+)$ as a probability distribution function for the variables α and α^+ , hence the name positive-P.

A hallmark of the PPR is that the off-diagonal projection operators, $\hat{\Lambda}(\alpha, \alpha^+)$ satisfies the following correspondence relations:

$$\begin{aligned} \hat{a}\hat{\Lambda} &= \alpha\hat{\Lambda} \\ \hat{a}^\dagger\hat{\Lambda} &= (\alpha^+ + \frac{\partial}{\partial\alpha})\hat{\Lambda} \\ \hat{\Lambda}\hat{a}^\dagger &= \alpha^+\hat{\Lambda} \\ \hat{\Lambda}\hat{a} &= (\alpha + \frac{\partial}{\partial\alpha^+})\hat{\Lambda}. \end{aligned} \quad (\text{A.3})$$

which allows us to map complicated operator equations consisting of bosonic annihilation and creation operators onto differential equations of phase space variables α, α^+ . The correspondence relation is typically used in an equation of motion for $\hat{\rho}$, which after integration by parts and ignoring of boundary terms, allows us to obtain a Fokker-Planck equation (FPE):

$$\frac{\partial P(\vec{x})}{\partial t} = \left\{ -\frac{\partial}{\partial x^\mu} A^\mu(\vec{x}) + \frac{1}{2} \frac{\partial}{\partial x^\mu} \frac{\partial}{\partial x^\nu} D^{\mu\nu}(\vec{x}) \right\} P(\vec{x}), \quad , \mu, \nu = 0 \dots N-1, \quad (\text{A.4})$$

where $\vec{x} = \{\vec{\alpha}, \vec{\alpha}^+\}$, A^μ is called the drift vector and $D^{\mu\nu}$ is called the diffusion matrix (which is symmetric and positive semi-definite by definition). Due to the doubling of phase space, the diffusion matrix is guaranteed to be positive semi-definite [24]. This then allows one to convert the FPE to a set of Ito SDEs proportional to the number of bosonic modes of the system, i.e.

$$dx^\mu = A^\mu dt + B^{\mu\nu} dW^\nu, \quad \mu = 0 \dots N-1, \nu = 0 \dots N_w, \quad (\text{A.5})$$

where dW^ν is a vector of Wiener increments with N_w components and $B^{\mu\nu}$ is a noise matrix that must satisfy the factorization

$$\mathbf{D} = \mathbf{B}\mathbf{B}^T. \quad (\text{A.6})$$

This factorization is not unique and any noise matrix that satisfies Eq. A.6 will produce the same stochastic averages in the limit of an infinite number of trajectories. This ambiguity in the choice of \mathbf{B} may affect the performance of stochastic simulations [36, 38].

Since $\mathbf{D} = \mathbf{D}^T$, an obvious factorization to use would be the square root of the diffusion matrix, i.e. $\mathbf{B} = \sqrt{\mathbf{D}}$, which is easily accomplished by using common mathematical software such as Matlab or Maple. While this is the most convenient procedure, it does not necessarily produce the most elegant noise matrix. On the other hand, it is possible to decompose a single diffusion matrix into different diffusion processes [38]: $\mathbf{D} = \mathbf{D}_1 + \mathbf{D}_2 + \mathbf{D}_3 + \dots$ that may be more easily factorized, i.e. the factorization $\mathbf{D}_i = \mathbf{B}_i\mathbf{B}_i^T$ is trivial. Using this procedure, an equivalent noise matrix that also results in \mathbf{D} is given by

$$\mathbf{B} = [\mathbf{B}_1 \ \mathbf{B}_2 \ \mathbf{B}_3 \ \dots]. \quad (\text{A.7})$$

Despite possibly taking on a more elegant form, Eq. A.7 introduces $N_w (> N)$ Wiener increments and with that the possibility of larger sampling errors. So we see that there are advantages and disadvantages of the two factorization methods.

The convenience in using the positive-P representation is in calculating the expectation values of normal-ordered operators as they can be replaced by simple stochastic averages over their corresponding phase space functions. The equivalence is as follows

$$\langle (\hat{a}^\dagger)^m (\hat{a})^n \rangle = \langle \langle (\alpha^+)^m (\alpha)^n \rangle \rangle \quad (\text{A.8})$$

where $\langle \cdot \rangle$ is the usual quantum mechanical expectation value and $\langle \langle \cdot \rangle \rangle$ represents an average over stochastic trajectories. In the limit that the number of trajectories goes to infinity, we get an exact correspondence, although an average over $10^4 - 10^6$ trajectories usually gives good agreement‡ before sampling errors cause divergences [35].

The main downside of the PPR is its notoriously short simulation life times. This is typically caused by instabilities in the drift or diffusion term [25] that cause trajectories to

‡ This is just a general observation of the number of trajectories used in different articles when applying the positive-P representation. See [28, 29, 33] for example.

diverge in a finite time, when a finite number of trajectories are used to calculate expectation values. With that being said, the positive-P representation is best used for systems where the interesting physics occur at short timescales. Nonetheless, this does not deter us from our current aim of demonstrating the possibility of simulating real time spin dynamics using SDES, even if only for short times.

Appendix B. Initial distribution

An important point in simulating SDES would be using the right initial values for the phase space variables, α, α^+ . For any density matrix, a particular form of the positive-P distribution function [24] that always exist is given by

$$P(\alpha, \alpha^+) = \frac{1}{4\pi^2} \langle (\alpha + (\alpha^+)^*)/2 | \hat{\rho} | (\alpha + (\alpha^+)^*)/2 \rangle e^{-|\alpha - (\alpha^+)^*|^2/4}. \quad (\text{B.1})$$

It has been shown in [51] that using Eq. B.1, it is possible to initialize the phase space variables for a variety of initial states such as: coherent states, fock states or crescent states to name a few. Of interest to us is the initial positive P-distribution for number states: $|n\rangle\langle n|$ which takes the form:

$$P(\mu, \gamma) = \frac{e^{-|\gamma|^2}}{\pi} \frac{\Gamma(|\mu|^2, n+1)}{\pi} \quad (\text{B.2})$$

where

$$\Gamma(x, n) = \frac{e^{-x} x^{n-1}}{(n-1)!} \quad (\text{B.3})$$

is the Gamma distribution. Our phase space variables are related to γ and μ via the relation $\alpha = \mu + \gamma$ and $\alpha^+ = \mu^* - \gamma^*$ and so by sampling γ and μ using the appropriate distribution functions in Eq. B.2 (i.e. gamma distribution for μ and gaussian distribution for γ), we can invert them to find the numerical values for α and α^+ that represents the fock state $|n\rangle\langle n|$. Although, we have only outlined the steps for initializing the distribution of a fock state, more explicit details can be found in the useful article in [51].

While in this paper, we initialise the system in either the FM ground state or the AFM, it is in principle possible to initialise the system in a general entangled state, which is described by the following density operator:

$$\hat{\rho} = \frac{1}{N} (w_1 |\uparrow\rangle + w_0 |\downarrow\rangle) (\langle\uparrow| w_1 + \langle\downarrow| w_0), \quad (\text{B.4})$$

where $N = w_0^2 + w_1^2$ and w_0 and w_1 represent the probabilities of the entangled state being spin down and spin up state respectively. Or in the language of \hat{a} and \hat{b} bosons:

$$\hat{\rho} = \frac{1}{N} (w_1 |1, 0\rangle + w_0 |0, 1\rangle) (\langle 1, 0| w_1 + \langle 0, 1| w_0). \quad (\text{B.5})$$

The general entangled state is of interest as it is the ground state of the random field Ising model (RFIM), which our formalism is also able to address. Substituting eq. B.5 into eq. B.1, the coherent state basis results in the following expression for the probability distribution:

$$P(\mu_{\bar{\alpha}}, \gamma_{\bar{\alpha}}, \mu_{\bar{\beta}}, \gamma_{\bar{\beta}}) = \frac{1}{N} \left[w_0^2 \Gamma(|\mu_{\bar{\alpha}}|^2, 2) \frac{e^{-|\gamma_{\bar{\alpha}}|^2}}{\pi} \delta(\mu_{\bar{\beta}}) + w_1^2 \delta(\mu_{\bar{\alpha}}) \Gamma(|\mu_{\bar{\beta}}|^2, 2) \frac{e^{-|\gamma_{\bar{\beta}}|^2}}{\pi} \right. \\ \left. w_0 w_1 \left(\frac{e^{-|\mu_{\bar{\alpha}}|^2} |\mu_{\bar{\alpha}}| e^{-|\gamma_{\bar{\alpha}}|^2}}{\pi} \right) \left(\frac{e^{-|\mu_{\bar{\beta}}|^2} |\mu_{\bar{\beta}}| e^{-|\gamma_{\bar{\beta}}|^2}}{\pi} \right) 2 \cos(2\eta) \right] \quad (\text{B.6})$$

where $\mu_{\bar{\alpha}} = |\mu_{\bar{\alpha}}| e^{i(\eta+\xi)} = |\mu_{\bar{\alpha}}| e^{i(\xi+\eta)}$ and $\mu_{\bar{\beta}} = |\mu_{\bar{\beta}}| e^{i(\eta+\xi)} = |\mu_{\bar{\beta}}| e^{i(\xi-\eta)}$. Note that we have made a similar change of variables as above, i.e.

$$\mu_{\bar{\alpha}} = \frac{\alpha + (\alpha^+)^*}{2}, \quad \gamma_{\bar{\alpha}} = \frac{\alpha - (\alpha^+)^*}{2} \\ \mu_{\bar{\beta}} = \frac{\beta + (\beta^+)^*}{2}, \quad \gamma_{\bar{\beta}} = \frac{\beta - (\beta^+)^*}{2} \quad (\text{B.7})$$

The PPR based on the SU-(n) coherent states [46] seems more tailored to dealing with superposition states, as they can be more easily initialized with delta functions.

Appendix C. Fokker-Planck Equation for Heisenberg Hamiltonian

If we were to apply formalism outlined in Appendix A, we obtain the following FPE for the TFIM in Eq. 3:

$$\frac{\partial P(\vec{\alpha}, \vec{\alpha}^+, \vec{\beta}, \vec{\beta}^+)}{dt} = \sum_i \left(-\frac{\partial}{\partial \alpha_i} \left\{ \frac{iJ}{4\hbar} \alpha_i \left[(n_{i+1}^\alpha - n_{i+1}^\beta) + (n_{i-1}^\alpha - n_{i-1}^\beta) \right] + \frac{i\hbar(t)}{2\hbar} \beta_i \right\} \right. \\ \left. - \frac{\partial}{\partial \alpha_i^+} \left\{ \frac{iJ}{4\hbar} \alpha_i^+ \left[(n_{i+1}^\beta - n_{i+1}^\alpha) + (n_{i-1}^\beta - n_{i-1}^\alpha) \right] - \frac{i\hbar(t)}{2\hbar} \beta_i^+ \right\} \right. \\ \left. - \frac{\partial}{\partial \beta_i} \left\{ \frac{iJ}{4\hbar} \beta_i \left[(n_{i+1}^\beta - n_{i+1}^\alpha) + (n_{i-1}^\beta - n_{i-1}^\alpha) \right] + \frac{i\hbar(t)}{2\hbar} \alpha_i \right\} \right. \\ \left. - \frac{\partial}{\partial \beta_i^+} \left\{ \frac{iJ}{4\hbar} \beta_i^+ \left[(n_{i+1}^\alpha - n_{i+1}^\beta) + (n_{i-1}^\alpha - n_{i-1}^\beta) \right] - \frac{i\hbar(t)}{2\hbar} \alpha_i^+ \right\} \right. \\ \left. + \frac{1}{2} \left(\frac{iJ}{4\hbar} \right) \left[\frac{\partial^2}{\partial \alpha_i \partial \alpha_{i+1}} \alpha_i \alpha_{i+1} + \frac{\partial^2}{\partial \alpha_{i+1} \partial \alpha_i} \alpha_i \alpha_{i+1} - \frac{\partial^2}{\partial \alpha_i^+ \partial \alpha_{i+1}^+} \alpha_i^+ \alpha_{i+1}^+ - \frac{\partial^2}{\partial \alpha_{i+1}^+ \partial \alpha_i^+} \alpha_i^+ \alpha_{i+1}^+ \right. \right. \\ \left. \frac{\partial^2}{\partial \beta_i \partial \beta_{i+1}} \beta_i \beta_{i+1} + \frac{\partial^2}{\partial \beta_{i+1} \partial \beta_i} \beta_i \beta_{i+1} - \frac{\partial^2}{\partial \beta_i^+ \partial \beta_{i+1}^+} \beta_i^+ \beta_{i+1}^+ - \frac{\partial^2}{\partial \beta_{i+1}^+ \partial \beta_i^+} \beta_i^+ \beta_{i+1}^+ \right. \\ \left. \frac{\partial^2}{\partial \alpha_i^+ \partial \beta_{i+1}^+} \alpha_i^+ \beta_{i+1}^+ + \frac{\partial^2}{\partial \beta_{i+1}^+ \partial \alpha_i^+} \alpha_i^+ \beta_{i+1}^+ + \frac{\partial^2}{\partial \alpha_{i+1}^+ \partial \beta_i^+} \alpha_{i+1}^+ \beta_i^+ + \frac{\partial^2}{\partial \beta_i^+ \partial \alpha_{i+1}^+} \alpha_{i+1}^+ \beta_i^+ \right. \\ \left. - \frac{\partial^2}{\partial \alpha_i \partial \beta_{i+1}} \alpha_i \beta_{i+1} - \frac{\partial^2}{\partial \beta_{i+1} \partial \alpha_i} \alpha_i \beta_{i+1} - \frac{\partial^2}{\partial \alpha_{i+1} \partial \beta_i} \alpha_{i+1} \beta_i \right]$$

$$\left. -\frac{\partial^2}{\partial\beta_i\partial\alpha_{i+1}}\alpha_{i+1}\beta_i \right] P(\vec{\alpha}, \vec{\alpha}^+, \vec{\beta}, \vec{\beta}^+) \quad (\text{C.1})$$

where we have already carried out an integration by parts and assumed that boundary terms vanish. By inspecting Eq. C.1, the diffusion matrix (which is a $4N \times 4N$ matrix), has matrix elements that are specified by the functions associated with their derivatives.

Obviously, calculating the noise matrix is not a trivial task and comprises the bulk of the analytical work. Instead of simply taking the straightforward $\mathbf{B} = \sqrt{\mathbf{D}}$ choice, we used the trick mentioned in Appendix A and decomposed our diffusion matrix into eight different constituents, i.e.:

$$\mathbf{D} = \mathbf{D}^\alpha + \mathbf{D}^\beta + \mathbf{D}^{\alpha^+} + \mathbf{D}^{\beta^+} + \mathbf{D}^{\beta\alpha} + \mathbf{D}^{\alpha\beta} + \mathbf{D}^{\beta^+\alpha^+} + \mathbf{D}^{\alpha^+\beta^+} \quad (\text{C.2})$$

where the obvious choice for these constituents would be

$$\begin{aligned} (\mathbf{D}^\alpha)_{i,i+1} &= (\mathbf{D}^\alpha)_{i+1,i} = \frac{iJ}{4\hbar}\alpha_i\alpha_{i+1} \\ (\mathbf{D}^\beta)_{i,i+1} &= (\mathbf{D}^\beta)_{i+1,i} = \frac{iJ}{4\hbar}\beta_i\beta_{i+1} \\ (\mathbf{D}^{\alpha^+})_{i,i+1} &= (\mathbf{D}^{\alpha^+})_{i+1,i} = -\frac{iJ}{4\hbar}\alpha_i^+\alpha_{i+1}^+ \\ (\mathbf{D}^{\beta^+})_{i,i+1} &= (\mathbf{D}^{\beta^+})_{i+1,i} = -\frac{iJ}{4\hbar}\beta_i^+\beta_{i+1}^+ \\ (\mathbf{D}^{\beta\alpha})_{i,i+1} &= (\mathbf{D}^{\beta\alpha})_{i+1,i} = -\frac{iJ}{4\hbar}\alpha_i\beta_{i+1} \\ (\mathbf{D}^{\alpha\beta})_{i,i+1} &= (\mathbf{D}^{\alpha\beta})_{i+1,i} = -\frac{iJ}{4\hbar}\beta_i\alpha_{i+1} \\ (\mathbf{D}^{\beta^+\alpha^+})_{i,i+1} &= (\mathbf{D}^{\beta^+\alpha^+})_{i+1,i} = \frac{iJ}{4\hbar}\alpha_i^+\beta_{i+1}^+ \\ (\mathbf{D}^{\alpha^+\beta^+})_{i,i+1} &= (\mathbf{D}^{\alpha^+\beta^+})_{i+1,i} = \frac{iJ}{4\hbar}\beta_i^+\alpha_{i+1}^+. \end{aligned}$$

The idea is that instead of factorizing one complicated diffusion matrix, \mathbf{D} we can instead factorize eight relatively simpler looking noise matrices, i.e. solving $\mathbf{B}^x (\mathbf{B}^x)^T = \mathbf{D}^x$. To make things slightly more transparent we will write out the general form for the first constituent, i.e. $x = \alpha$:

$$\mathbf{D}^\alpha = \frac{iJ}{4\hbar} \begin{bmatrix} \begin{bmatrix} 0 & \alpha_0\alpha_1 & 0 & \dots & t\alpha_0\alpha_{N-1} \\ \alpha_1\alpha_0 & 0 & \alpha_1\alpha_2 & \dots & 0 \\ 0 & \alpha_2\alpha_1 & 0 & \ddots & 0 \\ \vdots & 0 & \ddots & \dots & 0 \\ \alpha_{N-1}\alpha_0 & 0 & \dots & \dots & 0 \end{bmatrix} & \begin{bmatrix} \mathbf{0} & \mathbf{0} & \mathbf{0} \\ \mathbf{0} & \mathbf{0} & \mathbf{0} \\ \mathbf{0} & \mathbf{0} & \mathbf{0} \end{bmatrix} \end{bmatrix} \quad (\text{C.3})$$

where $\mathbf{0}$ represents an $N \times N$ null matrix. If it were possible to find \mathbf{B}^x for all x , then the total noise matrix takes the form of Eq. A.7.

Unfortunately, using the obvious choice $\sqrt{B^x}$ would still be messy and it would appear that we have not made things any easier. However, we can apply the same trick once more and decompose each \mathbf{D}^x into N subconstituents: $\{\mathbf{D}_j^x, j = 0 \dots N - 1\}$. Once again taking the $x = \alpha$ matrix as an example, the intuitive way of choosing the subconstituents is:

$$\mathbf{D}^\alpha = \mathbf{D}_0^\alpha + \mathbf{D}_1^\alpha + \dots + \mathbf{D}_{N-1}^\alpha \quad (\text{C.4})$$

$$= \frac{iJ}{4\hbar} \begin{bmatrix} 0 & \alpha_0\alpha_1 & \dots & \dots & 0 \\ \alpha_1\alpha_0 & 0 & \dots & \dots & \\ \vdots & \vdots & \ddots & \dots & \vdots \\ \vdots & \vdots & \ddots & \dots & \vdots \\ 0 & 0 & \dots & \dots & 0 \end{bmatrix} + \frac{iJ}{4\hbar} \begin{bmatrix} 0 & 0 & \dots & \dots & 0 \\ 0 & 0 & \alpha_1\alpha_2 & \dots & \\ 0 & \alpha_2\alpha_1 & \ddots & \dots & \\ \vdots & \vdots & \dots & \ddots & \vdots \\ 0 & \dots & \dots & \dots & 0 \end{bmatrix} + \dots \quad (\text{C.5})$$

$$+ \frac{iJ}{4\hbar} \begin{bmatrix} 0 & \dots & \dots & \dots & \alpha_0\alpha_{N-1} \\ 0 & \dots & \vdots & \dots & \\ \vdots & \dots & \ddots & \dots & \\ \vdots & \vdots & \dots & \ddots & \vdots \\ \alpha_{N-1}\alpha & \dots & \dots & \dots & 0 \end{bmatrix}$$

where the only non-trivial matrix elements of \mathbf{D}_j^α are given by

$$(\mathbf{D}_j^\alpha)_{i,i+1} = (\mathbf{D}_j^\alpha)_{i+1,i} = \frac{iJ}{4\hbar} \alpha_j \alpha_{j+1} \quad (\text{C.6})$$

Each subconstituent diffusion matrix \mathbf{D}_i^α can then be individually factorized. This reduces the original problem to the much more trivial problem of factorizing matrices of the following form:

$$\mathbf{D}' = \begin{bmatrix} 0 & X \\ X & 0 \end{bmatrix} \quad (\text{C.7})$$

for which we can easily show that either

$$\mathbf{B}' = \begin{bmatrix} -\sqrt{X/2} & -i\sqrt{X/2} \\ -\sqrt{X/2} & i\sqrt{X/2} \end{bmatrix} \quad (\text{C.8})$$

or

$$\mathbf{B}'' = \begin{bmatrix} -\sqrt{X/2} & i\sqrt{X/2} \\ -\sqrt{X/2} & -i\sqrt{X/2} \end{bmatrix} \quad (\text{C.9})$$

satisfies the necessary relation in Eq. A.6. Now, granted that the decomposition for each \mathbf{D}_i^α exists, we can write Eq. C.4 as:

$$\mathbf{D}^\alpha = \mathbf{B}_0^\alpha (\mathbf{B}_0^\alpha)^T + \mathbf{B}_1^\alpha (\mathbf{B}_1^\alpha)^T + \dots + \mathbf{B}_{N-1}^\alpha (\mathbf{B}_{N-1}^\alpha)^T \quad (\text{C.10})$$

so that according to Eq. A.7, the total noise matrix for \mathbf{D}^α takes the obvious form:

$$\mathbf{B}^\alpha = \left[\begin{array}{c|c|c|c|c|c} \mathbf{B}_0^\alpha & \mathbf{B}_1^\alpha & \dots & \mathbf{B}_j^\alpha & \dots & \mathbf{B}_{N-1}^\alpha \\ \hline \mathbf{B}_0^\alpha & \mathbf{B}_1^\alpha & \dots & \mathbf{B}_j^\alpha & \dots & \mathbf{B}_{N-1}^\alpha \\ \hline \mathbf{B}_0^\alpha & \mathbf{B}_1^\alpha & \dots & \mathbf{B}_j^\alpha & \dots & \mathbf{B}_{N-1}^\alpha \\ \hline \mathbf{B}_0^\alpha & \mathbf{B}_1^\alpha & \dots & \mathbf{B}_j^\alpha & \dots & \mathbf{B}_{N-1}^\alpha \\ \hline \mathbf{B}_0^\alpha & \mathbf{B}_1^\alpha & \dots & \mathbf{B}_j^\alpha & \dots & \mathbf{B}_{N-1}^\alpha \\ \hline \mathbf{B}_0^\alpha & \mathbf{B}_1^\alpha & \dots & \mathbf{B}_j^\alpha & \dots & \mathbf{B}_{N-1}^\alpha \end{array} \right] \quad (\text{C.11})$$

obviously satisfying Eq. A.6, with the only non-zero elements being:

$$\begin{aligned} (\mathbf{B}_j^\alpha)_{j,2j} &= -\frac{1}{2} \sqrt{\frac{iJ}{4\hbar}} \sqrt{\alpha_j \alpha_{j+1}} \\ (\mathbf{B}_j^\alpha)_{j,2j+1} &= -\frac{i}{2} \sqrt{\frac{iJ}{4\hbar}} \sqrt{\alpha_j \alpha_{j+1}} \\ (\mathbf{B}_j^\alpha)_{j+1,2j} &= -\frac{1}{2} \sqrt{\frac{iJ}{4\hbar}} \sqrt{\alpha_j \alpha_{j+1}} \\ (\mathbf{B}_j^\alpha)_{j+1,2j+1} &= \frac{i}{2} \sqrt{\frac{iJ}{4\hbar}} \sqrt{\alpha_j \alpha_{j+1}} \end{aligned}$$

where $j = 0 \dots N - 1$. As an explicit example, the $N = 4$ case of Eq. C.11 is shown below:

$$\mathbf{B}^\alpha = \frac{1}{2} \sqrt{\frac{iJ}{4\hbar}} \left[\begin{array}{c} \left[\begin{array}{cc} -\sqrt{\alpha_0 \alpha_1} & -i\sqrt{\alpha_0 \alpha_1} \\ -\sqrt{\alpha_0 \alpha_1} & +i\sqrt{\alpha_0 \alpha_1} \\ 0 & 0 \\ 0 & 0 \\ \vdots & \vdots \\ 0 & 0 \end{array} \right] \left[\begin{array}{cc} 0 & 0 \\ -\sqrt{\alpha_1 \alpha_2} & -i\sqrt{\alpha_1 \alpha_2} \\ -\sqrt{\alpha_1 \alpha_2} & i\sqrt{\alpha_1 \alpha_2} \\ 0 & 0 \\ \vdots & \vdots \\ 0 & 0 \end{array} \right] \left[\begin{array}{cc} 0 & 0 \\ 0 & 0 \\ -\sqrt{\alpha_2 \alpha_3} & -i\sqrt{\alpha_2 \alpha_3} \\ -\sqrt{\alpha_2 \alpha_3} & i\sqrt{\alpha_2 \alpha_3} \\ \vdots & \vdots \\ 0 & 0 \end{array} \right] \\ \left[\begin{array}{cc} -\sqrt{\alpha_0 \alpha_3} & -i\sqrt{\alpha_0 \alpha_3} \\ 0 & 0 \\ 0 & 0 \\ -\sqrt{\alpha_0 \alpha_3} & +i\sqrt{\alpha_0 \alpha_3} \\ \vdots & \vdots \\ 0 & 0 \end{array} \right] \end{array} \right] \quad (\text{C.12})$$

which is an $4N \times 2N$ matrix with most elements being trivial. This noise matrix would therefore introduce $2N$ independent Wiener increments (see Eq. A.5) can be stored as the components of the Wiener increment vector: $d\vec{W}^\alpha$. In this fashion, the noise terms for the

SDEs in Eq. 10 to Eq. 13 can be derived. If we label $d\vec{W}^\alpha$ in the conventional way^{††} then:

$$d\vec{W}^\alpha = \begin{bmatrix} dW_0^\alpha \\ dW_1^\alpha \\ \vdots \\ \vdots \\ dW_{N-1}^\alpha \end{bmatrix}, \quad (\text{C.14})$$

and the resulting stochastic terms only contribute to $d\vec{\alpha}$, i.e.:

$$d\alpha_i \propto -\sqrt{\alpha_i \alpha_{i+1}} (dW_{2i} + idW_{2i+1}) - \sqrt{\alpha_i \alpha_{i-1}} (dW_{2i-2} + idW_{2i-1}). \quad (\text{C.15})$$

where we assumed "periodic boundary conditions" for the Wiener increment vectors in the sense that $dW_{-i} = dW_{N-i}$ where $i \in [0, N - 1]$.

Acknowledgments

This research has been made possible with the support of an NSERC research grant. We would also like to thank Piotr Deuar and Murray Olsen for helpful discussions.

References

- [1] P Calabrese and J Cardy. Quantum quenches in extended systems. Journal of Statistical Mechanics: Theory and Experiment, 2007:P06008, 2007.
- [2] P Calabrese and J Cardy. Entanglement and correlation functions following a local quench: a conformal field theory approach. Journal of Statistical Mechanics: Theory and Experiment, 2007:P10004, 2007.
- [3] C Kollath, AM Läuchli, and E Altman. Quench dynamics and nonequilibrium phase diagram of the bose-hubbard model. Physical review letters, 98(18):180601, 2007.
- [4] S. R. Manmana, S. Wessel, R. M. Noack, and A. Muramatsu. Strongly correlated fermions after a quantum quench. Phys. Rev. Lett., 98(21):210405, May 2007.
- [5] P Barmettler, M Punk, V Gritsev, E Demler, and E Altman. Relaxation of antiferromagnetic order in spin-1/2 chains following a quantum quench. Physical review letters, 102(13):130603, 2009.
- [6] G Roux. Quenches in quantum many-body systems: One-dimensional bose-hubbard model reexamined. Physical Review A, 79(2):21608, 2009.
- [7] S Langer, F Heidrich-Meisner, J Gemmer, IP McCulloch, and U Schollwöck. Real-time study of diffusive and ballistic transport in spin-1/2 chains using the adaptive time-dependent density matrix renormalization group method. Phys. Rev. B, 79(21):214409, 2009.
- [8] Guillaume Roux. Finite-size effects in global quantum quenches: Examples from free bosons in an harmonic trap and the one-dimensional bose-hubbard model. Phys. Rev. A, 81(5):053604, May 2010.
- [9] Peter Barmettler, Matthias Punk, Vladimir Gritsev, Eugene Demler, and Ehud Altman. Quantum quenches in the anisotropic spin-1/2 heisenberg chain: different approaches to many-body dynamics far from equilibrium. New Journal of Physics, 12(5):055017, 2010.

^{††}The labeling for $dW^{\alpha\beta}$, $dW^{\beta\alpha}$, $dW^{\beta^+\alpha^+}$ and $dW^{\alpha^+\beta^+}$ does not follow the usual convention and can be deduced from the corresponding noise terms in Eq. 10 to Eq. 13

- [10] Toma Prosen. Third quantization: a general method to solve master equations for quadratic open fermi systems. New Journal of Physics, 10(4):043026, 2008.
- [11] Pasquale Calabrese Alexandre Faribault and Jean-Sbastien Caux. Bethe ansatz approach to quench dynamics in the richardson model. Journal of Mathematical Physics, 50:095212, 2009.
- [12] Alexandre Faribault, Pasquale Calabrese, and Jean-Sbastien Caux. Quantum quenches from integrability: the fermionic pairing model. Journal of Statistical Mechanics: Theory and Experiment, 2009(03):P03018, 2009.
- [13] Matteo Rizzi, Simone Montangero, and Guifre Vidal. Simulation of time evolution with multiscale entanglement renormalization ansatz. Phys. Rev. A, 77(5):052328, May 2008.
- [14] Davide Fioretto and Giuseppe Mussardo. Quantum quenches in integrable field theories. New Journal of Physics, 12(5):055015, 2010.
- [15] Maurizio Fagotti and Pasquale Calabrese. Evolution of entanglement entropy following a quantum quench: Analytic results for the xy chain in a transverse magnetic field. Phys. Rev. A, 78(1):010306, Jul 2008.
- [16] AJ Daley, C Kollath, U Schollwöck, and G Vidal. Time-dependent density-matrix renormalization-group using adaptive effective hilbert spaces. Journal of Statistical Mechanics: Theory and Experiment, 2004:P04005, 2004.
- [17] SR White and AE Feiguin. Real-time evolution using the density matrix renormalization group. Physical review letters, 93(7):76401, 2004.
- [18] MC Bañuls, MB Hastings, F Verstraete, and JI Cirac. Matrix product states for dynamical simulation of infinite chains. Physical review letters, 102(24):240603, 2009.
- [19] D Gobert, C Kollath, U Schollwoeck, and G Schuetz. Real-time dynamics in spin-1/2 chains with adaptive time-dependent density matrix renormalization group. Physical Review E, 71(3):36102, 2005.
- [20] F. Verstraete, J. J. García-Ripoll, and J. I. Cirac. Matrix product density operators: Simulation of finite-temperature and dissipative systems. Phys. Rev. Lett., 93(20):207204, Nov 2004.
- [21] M Zwolak and G Vidal. Mixed-state dynamics in one-dimensional quantum lattice systems: a time-dependent superoperator renormalization algorithm. Physical review letters, 93(20):207205, 2004.
- [22] Michael J Hartmann, Javier Prior, Stephen R Clark, and Martin B Plenio. Density matrix renormalization group in the heisenberg picture. Physical review letters, 102(5):057202, Jan 2009.
- [23] S. R Clark, J Prior, M. J Hartmann, D Jaksch, and M. B Plenio. Exact matrix product solutions in the heisenberg picture of an open quantum spin chain. New J Phys, 12:025005, Jan 2010.
- [24] P D Drummond and C W Gardiner. Generalised p-representations in quantum optics. Journal of Physics A: Mathematical and General, 13(7):2353, 1980.
- [25] P. Deuar and P. D. Drummond. Gauge p representations for quantum-dynamical problems: Removal of boundary terms. Phys. Rev. A, 66(3):033812, Sep 2002.
- [26] H. Van Dam L. C. Biedenharn, editor. Quantum Theory of Angular Momentun. Academic Press, 1965.
- [27] J. J. Sakurai. Modern Quantum Mechanics. Addison-Wesley, 1994.
- [28] M.K. Olsen, L.I. Plimak, S. Rebic, and A.S. Bradley. Phase-space analysis of bosonic spontaneous emission. Optics Communications, 254(4-6):271 – 281, 2005.
- [29] A. M. Smith and C. W. Gardiner. Simulations of nonlinear quantum damping using the positive p representation. Phys. Rev. A, 39(7):3511–3524, Apr 1989.
- [30] K. J. McNeil and I. J. D. Craig. Positive- p representation for second-harmonic generation: Analytic and computational results. Phys. Rev. A, 41(7):4009–4018, Apr 1990.
- [31] M. J. Steel, M. K. Olsen, L. I. Plimak, P. D. Drummond, S. M. Tan, M. J. Collett, D. F. Walls, and R. Graham. Dynamical quantum noise in trapped bose-einstein condensates. Phys. Rev. A, 58(6):4824–4835, Dec 1998.
- [32] P Deuar and P D Drummond. First-principles quantum dynamics in interacting bose gases: I. the

- positive p representation. Journal of Physics A: Mathematical and General, 39(5):1163, 2006.
- [33] P. Deuar and P. D. Drummond. Correlations in a bec collision: First-principles quantum dynamics with 150 000 atoms. Phys. Rev. Lett., 98(12):120402, Mar 2007.
 - [34] P. D. Drummond and I. K. Mortimer. Computer simulations of multiplicative stochastic differential equations. Journal of Computational Physics, 93(1):144 – 170, 1991.
 - [35] A. Gilchrist, C. W. Gardiner, and P. D. Drummond. Positive p representation: Application and validity. Phys. Rev. A, 55(4):3014–3032, Apr 1997.
 - [36] L. I. Plimak, M. K. Olsen, and M. J. Collett. Optimization of the positive- p representation for the anharmonic oscillator. Phys. Rev. A, 64(2):025801, Jul 2001.
 - [37] P. Deuar and P. D. Drummond. First-principles quantum dynamics in interacting bose gases ii: stochastic gauges. Journal of Physics A: Mathematical and General, 39(11):2723, 2006.
 - [38] P. Deuar. First-principles quantum simulations of many-mode open interacting Bose gases using stochastic gauge methods. ArXiv Condensed Matter e-prints, July 2005.
 - [39] P. Deuar and P. D. Drummond. Stochastic gauges in quantum dynamics for many-body simulations. Computer Physics Communications, 142(1-3):442 – 445, 2001.
 - [40] P. D. Drummond and P. Deuar. Quantum dynamics with stochastic gauge simulations. Journal of Optics B: Quantum and Semiclassical Optics, 5(3):S281, 2003.
 - [41] P. D. Drummond, P. Deuar, and K. V. Kheruntsyan. Canonical bose gas simulations with stochastic gauges. Phys. Rev. Lett., 92(4):040405, Jan 2004.
 - [42] S. Ghanbari, J. F. Corney, and T. D. Kieu. Finite temperature correlations in the Bose-Hubbard model: application of the Gauge- P representation. ArXiv e-prints, February 2010.
 - [43] P. Deuar, A. G. Sykes, D. M. Gangardt, M. J. Davis, P. D. Drummond, and K. V. Kheruntsyan. Nonlocal pair correlations in the one-dimensional bose gas at finite temperature. Phys. Rev. A, 79(4):043619, Apr 2009.
 - [44] I. Carusotto, Y. Castin, and J. Dalibard. n -boson time-dependent problem: A reformulation with stochastic wave functions. Phys. Rev. A, 63(2):023606, Jan 2001.
 - [45] Takeshi Aimi and Masatoshi Imada. Does simple two-dimensional hubbard model account for high- t_c superconductivity in copper oxides? Journal of the Physical Society of Japan, 76(11):113708, 2007.
 - [46] D. W. Barry and P. D. Drummond. Qubit phase space: $su(n)$ coherent-state p representations. Phys. Rev. A, 78(5):052108, Nov 2008.
 - [47] P. D. Drummond and J. F. Corney. Quantum dynamics of evaporatively cooled bose-einstein condensates. Phys. Rev. A, 60(4):R2661–R2664, Oct 1999.
 - [48] Magnus Ögren and K. V. Kheruntsyan. Atom-atom correlations in colliding bose-einstein condensates. Phys. Rev. A, 79(2):021606, Feb 2009.
 - [49] Klaus Mølmer, A. Perrin, V. Krachmalnicoff, V. Leung, D. Boiron, A. Aspect, and C. I. Westbrook. Hanbury brown and twiss correlations in atoms scattered from colliding condensates. Phys. Rev. A, 77(3):033601, Mar 2008.
 - [50] Roy J. Glauber. The quantum theory of optical coherence. Phys. Rev., 130(6):2529–2539, Jun 1963.
 - [51] M.K. Olsen and A.S. Bradley. Numerical representation of quantum states in the positive- p and wigner representations. Optics Communications, 282(19):3924 – 3929, 2009.